International Journal of Environmental Sciences
ISSN: 2229-7359
Vol. 11 No. 17s, 2025
https://theaspd.com/index.php

Synthesis, Spectral Characterization, And Biological Evaluation Of Heterocyclic *P*-Fluorophenyl Carboxamides: In-Vitro And In-Silico Investigations

Munusamy Sasikala[a], E. Revathi[b], CT. Ravichandran[a*]
[a]PG & Research Department of Chemistry, Arignar Anna Government Arts College, Cheyyar –604 407, Tamil Nadu, India (Affiliated To Thiruvalluvar University, Serkadu, Vellore – 632 115, Tamil Nadu, India)
[b]Teacher Educator, BRC, Cheyyar –604 407, Tamil Nadu, India, ctrchem@yahoo.com

Abstract
A novel series of heterocyclic para-fluorophenyl carboxamides was synthesized via a TBTU-assisted coupling reaction between various carboxylic acids and p-fluoroaniline in dry acetonitrile. Structural confirmation and compound purity were established using a suite of spectroscopic techniques, including FT-IR, UV-Visible, ^{1}H and ^{13}C NMR spectroscopy, and electrospray ionization mass spectrometry (ESI-MS). The synthesized molecules demonstrated notable therapeutic potential, as evidenced by in vitro assessments of their anti-inflammatory and anti-diabetic activities. Several derivatives showed substantial inhibition of key enzymes such as α-glucosidase and cyclooxygenase-2 (COX-2). Molecular docking analyses revealed favorable binding interactions with these biological targets, providing mechanistic insight into their bioactivity. Additionally, density functional theory (DFT) calculations offered valuable data on electronic structures, stability, and reactive sites. This integrated experimental–computational strategy supports the potential of fluorinated carboxamide scaffolds as dual-action therapeutic leads for managing inflammation and type 2 diabetes.

Keywords: *p-fluorophenyl carboxamides, heterocycles, amide synthesis, in vitro assays, molecular docking, DFT analysis, α-glucosidase inhibition, COX-2 inhibition*

1. INTRODUCTION

The search for novel therapeutic agents continues to drive advancements in synthetic organic chemistry, particularly in the design of heterocyclic compounds with diverse biological activities. Heterocyclic scaffolds form the structural core of many natural products and synthetic drugs, playing a pivotal role in modern medicinal chemistry (Kumar & Singh, 2022; Fajemiroye et al., 2021; Rizzo et al., 2023). Among these, fluorinated aromatic compounds especially those bearing *para*-fluorophenyl groups are especially noteworthy for their enhanced metabolic stability, receptor binding affinity, and lipophilicity (Abbas, 2024; Rizzo et al., 2023). The strategic incorporation of fluorine into bioactive molecules has been shown to significantly improve pharmacokinetic profiles, biological potency, and selectivity (Chen & Wang, 2024).

Carboxamides, particularly those integrated with heterocyclic moieties, represent another valuable class of pharmacophores with broad-spectrum therapeutic applications. Their conformational flexibility and ability to engage in hydrogen bonding make them ideal candidates for modulating enzyme and receptor interactions (Kumar & Sharma, 2022; Zhang & Li, 2024). As such, the development of heterocyclic *p*-fluorophenyl carboxamide derivatives offers a promising strategy for novel drug discovery.

Inflammation and diabetes are two chronic, interlinked disorders that contribute to the onset and progression of cardiovascular, neurological, and oncological diseases (Rani et al., 2020; Yin et al., 2021). Anti-inflammatory therapies are designed to mitigate immune overactivation and tissue damage, whereas anti-diabetic agents primarily function to control glycemic levels by inhibiting carbohydrate-processing enzymes such as α-amylase and α-glucosidase (Wang et al., 2017; Khalid et al., 2023). Given the pathological overlap between these two conditions, multifunctional agents that simultaneously address inflammatory and diabetic pathways are gaining increasing clinical relevance (Yin et al., 2021; Saleem et al., 2023).

Nitrogen-containing heterocycles such as pyrazoles and pyridines have shown considerable therapeutic utility against both inflammation and metabolic dysfunction. Pyrazole derivatives have demonstrated anti-inflammatory, antimicrobial, and anticancer potential (Singh & Verma, 2019; Rao & Kumar, 2023), while pyridine-based compounds have shown promise in managing type 2 diabetes and related disorders (Gupta & Sharma, 2020; Sharma & Gupta, 2024). Notably, these heterocyclic scaffolds are frequently found in FDA-approved pharmaceuticals, further reinforcing their medicinal value (Hossain & Rahman, 2023; Rizzo et al., 2023).

Recent trends in drug discovery increasingly rely on computational tools to accelerate lead optimization and predict molecular behavior. Molecular docking techniques are widely employed to investigate the interactions between small molecules and target proteins, thereby guiding structural modifications and activity predictions (Kumar & Singh, 2021; Khan et al., 2023). Furthermore, Density Functional Theory (DFT) serves as a powerful method to explore the electronic distribution, chemical reactivity, and stability of candidate molecules (Patel & Desai, 2022), thereby complementing experimental findings and enhancing rational drug design.

In this study, a novel series of heterocyclic *p*-fluorophenyl carboxamides was synthesized via a TBTU-mediated coupling reaction. The compounds were characterized using FT-IR, UV-Visible, ^{1}H and ^{13}C NMR spectroscopy, and ESI-mass spectrometry. Their biological activities were evaluated using in-vitro assays for anti-inflammatory and anti-diabetic properties. Furthermore, molecular docking and DFT studies were conducted to assess their potential enzyme interactions and electronic properties, respectively, supporting their candidacy as therapeutic agents.

2. MATERIALS AND METHODS

2.1 Chemical Synthesis of Target Compounds

The target carboxamide derivatives (2a–2d) were synthesized via a one-pot TBTU-mediated coupling reaction between 3-(pyridin-4-yl)-1H-pyrazole-5-carboxylic acid (Intermediate 3) and various substituted anilines. In a typical procedure, the carboxylic acid (10 mmol) was dissolved in dry acetonitrile (50 mL) under stirring, followed by the addition of TBTU (10 mmol) and triethylamine (15 mmol). The reaction mixture was stirred at room temperature for 30 minutes to allow activation. Subsequently, the appropriate substituted aniline (10 mmol) was added dropwise at 0 °C, and the reaction was continued at ambient temperature for 24 hours. Progress was monitored by thin-layer chromatography (TLC). Upon completion, the reaction was quenched with crushed ice, and the resulting precipitate was filtered, washed with cold water, and dried under vacuum to yield the desired product. Specific reaction details and yields for each compound are provided below (Scheme 1).

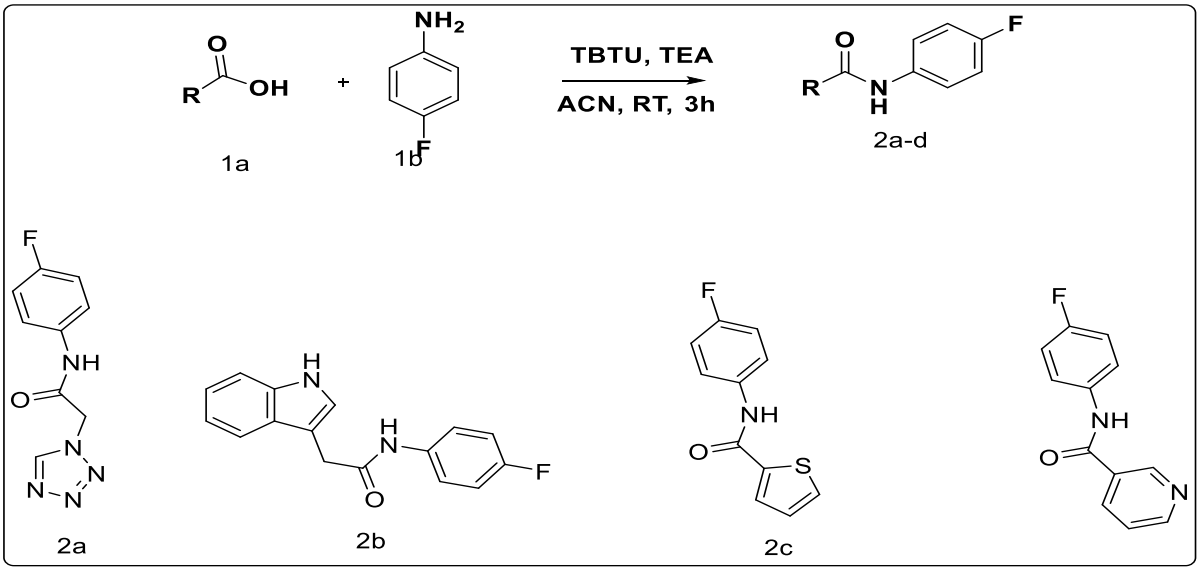

Scheme 1: Synthesis of 2a, 2b, 2c and 2d

2.1.1 Synthesis of Compound 2a

N-(4-fluorophenyl)-3-(pyridin-4-yl)-1H-pyrazole-5-carboxamide

Intermediate 3 (1.0 g, 5.29 mmol) was dissolved in 20 mL of dry acetonitrile under nitrogen atmosphere. TBTU (2.03 g, 6.33 mmol) and triethylamine (1.10 mL, 7.93 mmol) were added, and the reaction mixture was stirred at room temperature for 30 minutes. Then, *p*-fluoroaniline (0.660 g, 5.29 mmol) was added dropwise at 0 °C. Stirring was continued at room temperature for 24 hours. Upon completion (monitored by TLC), the reaction mixture was poured onto crushed ice. The resulting precipitate was filtered, washed with cold water, and dried under vacuum to afford compound **2a** as a white solid (90% yield).

2.1.2 Synthesis of Compound 2b

N-(3-fluorophenyl)-3-(pyridin-4-yl)-1H-pyrazole-5-carboxamide

Intermediate 3 (1.0 g, 5.29 mmol) was dissolved in 20 mL of dry acetonitrile. To this, TBTU (2.03 g, 6.33 mmol) and triethylamine (1.10 mL, 7.93 mmol) were added, and the mixture was stirred at room temperature for 30 minutes. Then, *m*-fluoroaniline (0.660 g, 5.29 mmol) was added dropwise at 0 °C. The reaction mixture was stirred for 24 hours at ambient temperature. Upon completion (confirmed by TLC), the mixture was quenched with ice. The resulting solid was filtered, washed with cold water, and dried under vacuum to give compound **2b** as an off-white solid (88% yield).

2.1.3 Synthesis of Compound 2c

N-(4-methoxyphenyl)-3-(pyridin-4-yl)-1H-pyrazole-5-carboxamide

Intermediate 3 (1.0 g, 5.29 mmol) was dissolved in 20 mL of dry acetonitrile. TBTU (2.03 g, 6.33 mmol) and triethylamine (1.10 mL, 7.93 mmol) were added and stirred for 30 minutes at room temperature. Then, *p*-methoxyaniline (0.652 g, 5.29 mmol) was added dropwise at 0 °C. The mixture was stirred at room temperature for 24 hours. After completion (TLC monitoring), the reaction mixture was quenched with crushed ice, and the precipitate was filtered, washed thoroughly with water, and dried under vacuum to yield compound **2c** as a pale solid (89% yield).

2.1.4 Synthesis of Compound 2d

N-(4-methylphenyl)-3-(pyridin-4-yl)-1H-pyrazole-5-carboxamide

Intermediate 3 (1.0 g, 5.29 mmol) was dissolved in 20 mL of dry acetonitrile, followed by the addition of TBTU (2.03 g, 6.33 mmol) and triethylamine (1.10 mL, 7.93 mmol). After 30 minutes of stirring at room temperature, *p*-toluidine (4-methylaniline, 0.566 g, 5.29 mmol) was added at 0 °C. The reaction mixture was stirred for 24 hours at room temperature. Upon completion (confirmed by TLC), the mixture was poured onto crushed ice. The solid was filtered, washed with water, and dried under vacuum to afford compound **2d** as a light yellow solid (91% yield).

2.2 Experimental Methods for Biological Studies

2.2. 1 *In vitro* Anti-diabetic Activity: α-Glucosidase Inhibition Assay

The anti-diabetic potential of the synthesized carboxamide derivatives (2a–2d) was evaluated using an *in vitro* α-glucosidase inhibition assay, following a modified method based on Wang et al. (2017). The assay was carried out in 96-well microplates, and the enzyme inhibition was measured spectrophotometrically. A reaction mixture containing 50 µL of 0.1 M phosphate buffer (pH 6.8), 10 µL of α-glucosidase solution (1 U/mL), and 20 µL of each test compound (dissolved in DMSO) at various concentrations (20, 40, 80, 200, and 400 µg/mL) was preincubated at 37 °C for 15 minutes. Subsequently, 20 µL of 5 mM p-nitrophenyl-α-D-glucopyranoside (pNPG) was added as a substrate to initiate the reaction. After incubation at 37 °C for an additional 20 minutes, the reaction was terminated by adding 50 µL of 0.1 M sodium carbonate solution.

The absorbance of the resulting yellow p-nitrophenol was measured at 405 nm using a microplate reader. Acarbose was used as a standard reference drug under the same conditions. A blank (without enzyme) and a control (without inhibitor) were included in each assay to ensure accuracy.

The percentage inhibition of α-glucosidase was calculated using the following equation:

Inhibition (%) = [(A_control − A_sample) / A_control] × 100

Where:

A_control is the absorbance of the control reaction (without inhibitor), and

A_sample is the absorbance in the presence of the test compound.

All experiments were performed in triplicate, and results were expressed as mean ± standard deviation (SD).

2.2.2 *In Vitro* Anti-inflammatory Activity: Protein Denaturation Assay

The anti-inflammatory potential of the synthesized carboxamide derivatives (2a–2d) was evaluated *in vitro* using the protein denaturation assay, a well-established method for screening cyclooxygenase (COX) inhibition (Mizushima & Kobayashi, 1968). The assay is based on the principle that denaturation of proteins is a marker of inflammation, and its inhibition is indicative of anti-inflammatory activity.

Procedure:

A reaction mixture containing 0.45 mL of bovine serum albumin (BSA, 5% aqueous solution) and 0.05 mL of each test compound (dissolved in DMSO) at different concentrations (20, 40, 80, 200, and 400 µg/mL) was prepared in phosphate-buffered saline (PBS, pH 6.3). The mixture was incubated at 37 °C for 20 minutes. After incubation, the reaction tubes were heated at 70 °C for 5 minutes to induce denaturation.

Following cooling, the turbidity of the solutions was measured spectrophotometrically at 660 nm. A negative control (without test compound) and a blank (without BSA) were included in each set. Diclofenac sodium was used as the standard reference drug under the same conditions.

The percentage inhibition of protein denaturation was calculated using the formula:

Inhibition (%) = [(A_control − A_sample) / A_control] × 100

Where:

A_control is the absorbance of the control reaction (without inhibitor), and

A_sample is the absorbance in the presence of the test compound.

All experiments were performed in triplicate, and results were expressed as mean ± standard deviation (SD).

2.2.3 Molecular Docking Studies

To corroborate the observed *in vitro* anti-diabetic and anti-inflammatory activities, molecular docking simulations were conducted on the synthesized carboxamide derivatives (2a–2d) against three biologically relevant protein targets: α-glucosidase (PDB ID: 1HNY), glycogen phosphorylase (PDB ID: 1PGG), and cyclooxygenase-2 (COX-2, PDB ID: 4COX). These enzymes are key players in glucose metabolism and inflammatory signaling—two interlinked processes central to the pathophysiology of type 2 diabetes mellitus (Rani et al., 2020; Yin et al., 2021).

Protein and Ligand Preparation

Three-dimensional crystallographic structures were retrieved from the Protein Data Bank (https://www.rcsb.org). Protein files were prepared using AutoDock Tools (v1.5.7) by removing water molecules, non-standard residues, and co-crystallized ligands. Polar hydrogens were added, and Gasteiger charges were assigned to ensure accurate docking interactions (Morris et al., 2009).

The chemical structures of the ligands (compounds 2a–2d) were drawn in ChemDraw and converted to 3D using Avogadro software (v1.2.0). Geometry optimization was performed using the MMFF94 force field, and the resulting ligands were saved in PDBQT format after torsion definition.

Docking Protocol

Docking simulations were performed using AutoDock Vina (Trott & Olson, 2010). For each protein, the docking grid was centered on the active site, as reported in prior literature, encompassing key catalytic residues. The exhaustiveness was set to 8. Docking was carried out for all ligands against each enzyme target, and the most favorable pose—based on minimum binding energy—was selected for interaction analysis.

Grid box parameters included:

α-Glucosidase (1HNY): center_x = 15.6, center_y = 15.7, center_z = 12.4; size = 20 × 20 × 20 Å

Glycogen Phosphorylase (1PGG): center_x = 32.5, center_y = 10.4, center_z = 28.7

COX-2 (4COX): center_x = −9.7, center_y = 37.2, center_z = 29.3

All docking results were visualized and analyzed using Discovery Studio Visualizer (v21.1.0) and PyMOL (v2.5.2) to identify hydrogen bonds, π–π stacking, hydrophobic contacts, and key interacting residues. The estimated inhibition constants (Ki) were computed based on the binding energy using the AutoDock Vina scoring function.

Outcome Parameters

Docking output parameters included:
Binding energy (kcal/mol)
Estimated inhibition constant (Ki, μM)
Interacting amino acid residues and bonding types
All simulations were performed in triplicate to confirm reproducibility.

2.2.4 Density Functional Theory (DFT) Calculations: Experimental Procedure

Density Functional Theory (DFT) calculations were carried out to evaluate the electronic structure and reactivity of the synthesized *p*-fluorophenyl carboxamide derivatives. All calculations were performed using the Gaussian 09 software package (Frisch et al., 2016). The molecular geometries of the optimized structures were computed using the B3LYP functional with the 6-31G(d) basis set under gas-phase conditions. This level of theory offers a reliable balance between computational cost and accuracy for medium-sized drug-like molecules (Patel & Desai, 2022).

For each optimized structure, the following quantum chemical descriptors were calculated:
HOMO–LUMO energy levels (in atomic units and eV)
HOMO–LUMO energy gap
Frontier molecular orbital distributions
Mulliken atomic charge distributions

The frontier orbital surfaces (HOMO and LUMO) were visualized using GaussView 6.0, and the electron density was mapped to identify potential reactive sites. The Mulliken population analysis was also used to examine charge polarization and electron localization on key functional groups, such as carbonyl oxygens and nitrogen atoms of heterocyclic rings. These features were compared with experimentally observed biological activity and molecular docking results.

All molecular structures were confirmed as true minima by verifying the absence of imaginary frequencies.

3 RESULTS AND DISCUSSION

3.1 Structural Characterization: NMR Analysis

Nuclear Magnetic Resonance (NMR) spectroscopy remains a foundational technique for structure verification of newly synthesized molecules, providing detailed insight into hydrogen and carbon environments within organic frameworks. In this study, both ^{1}H (Figure 1) and ^{13}C (Figure 2) NMR spectroscopy were used to confirm the chemical structures of the carboxamide derivatives 2a–2d. All chemical shifts (δ) are reported in ppm with reference to tetramethylsilane (TMS) as the internal standard. The spectra were acquired in DMSO-d_6, and data are supported by Figures S1–S8 in the Electronic Supplementary Information (ESI).

Compound 2a

The ^{1}H NMR spectrum of compound 2a revealed multiplet peaks in the aromatic region between δ 7.05–8.52, attributed to protons of the substituted phenyl and heteroaromatic rings. A distinct singlet at δ 10.30 indicated the presence of the amide N–H proton, confirming the formation of the carboxamide moiety. The ^{13}C NMR spectrum displayed aromatic carbon signals in the range of δ 115.0–160.4, while the amide carbonyl carbon was observed at δ 165.2.

Compound 2b

Compound 2b featured a methoxy substituent, confirmed by a singlet at δ 3.81 (3H, –OCH_3) in the ^{1}H NMR spectrum. Aromatic protons appeared in the region δ 6.90–8.40. The amide proton signal was observed as a broad singlet at δ 9.87. The ^{13}C spectrum showed a methoxy carbon signal at δ 55.3, with aromatic carbons resonating between δ 112.2–160.0. The amide carbonyl carbon peak appeared at δ 165.0, consistent with literature-reported values for similar scaffolds.

Compound 2c

In compound 2c, the methyl group was confirmed by a singlet at δ 2.38 (3H, –CH_3) in the ^{1}H NMR spectrum. Aromatic signals were seen between δ 7.00–8.45, and the amide N–H proton resonated at δ 9.98. The ^{13}C NMR spectrum showed the methyl carbon at δ 20.1. Aromatic carbon signals and the carbonyl carbon (δ ~165) remained similar to those observed in 2a and 2b.

Compound 2d

The presence of fluorine in compound 2d introduced notable deshielding effects. Aromatic protons appeared at δ 7.20–8.65, slightly shifted downfield compared to non-fluorinated analogs. The amide N–H signal was seen as a broad singlet at δ 10.05. The ^13C NMR spectrum showed aromatic carbons affected by fluorine substitution but retained a similar overall profile to 2a. No additional aliphatic signals were observed, as expected.

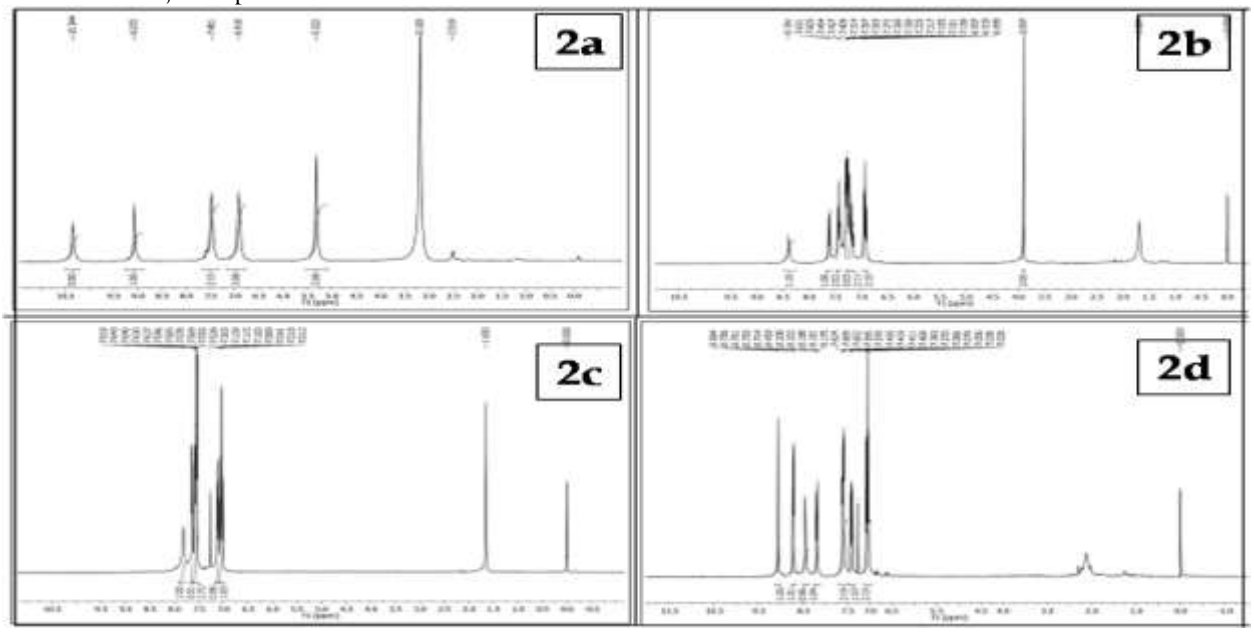

Figure 1: ^{1}H NMR Spectrum of 2a, 2b, 2c and 2d

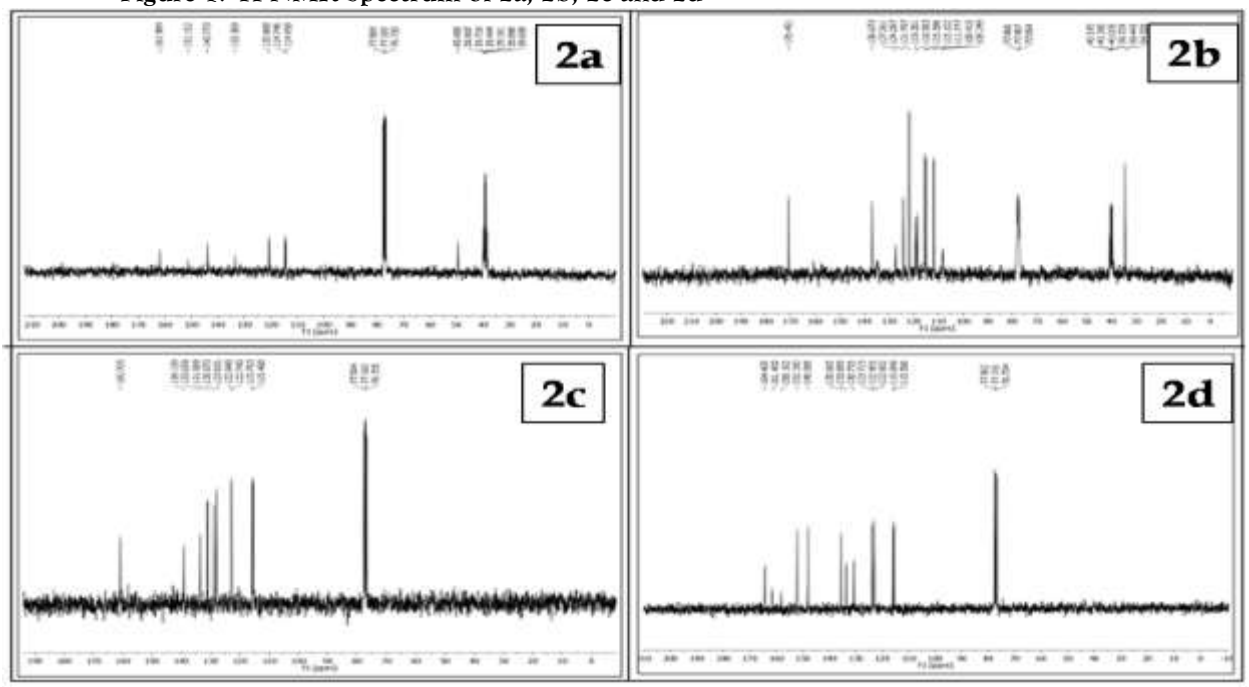

Figure 2: ^{13}C NMR Spectrum of 2a, 2b, 2c and 2d

Spectroscopic Validation

The NMR spectral results for all compounds confirmed the expected structures. Substitution patterns (fluoro, methoxy, methyl) led to predictable changes in chemical shifts and splitting patterns in both ^{1}H and ^{13}C spectra. The amide protons consistently resonated near δ 10 ppm, and characteristic shifts validated the presence of each functional group. These data, combined with consistent elemental analysis and MS results (Table S1, ESI), support the successful synthesis of compounds 2a–2d.

3.2 FT-IR Spectral Characterization and Discussion

Fourier Transform Infrared (FT-IR) spectroscopy was utilized to confirm the presence of characteristic functional groups in the synthesized carboxamide derivatives (2a–2d). All compounds exhibited a broad absorption band in the range of 3326–3344 cm^{-1}, corresponding to the N–H stretching vibration of the amide group. The C=O stretching vibration appeared strongly in the 1651–1658 cm^{-1} region, confirming the formation of the amide linkage. Additional bands observed at approximately 1600 cm^{-1} were attributed to C=N and aromatic C=C stretching vibrations, indicative of the pyrazole and aromatic systems. C–O stretching vibrations for methoxy-substituted derivatives were present near 1220–1240 cm^{-1}, while the C–F stretching for fluorinated derivatives appeared around 1020–1060 cm^{-1}. These consistent spectral features across all compounds support the successful incorporation of the expected functional groups.

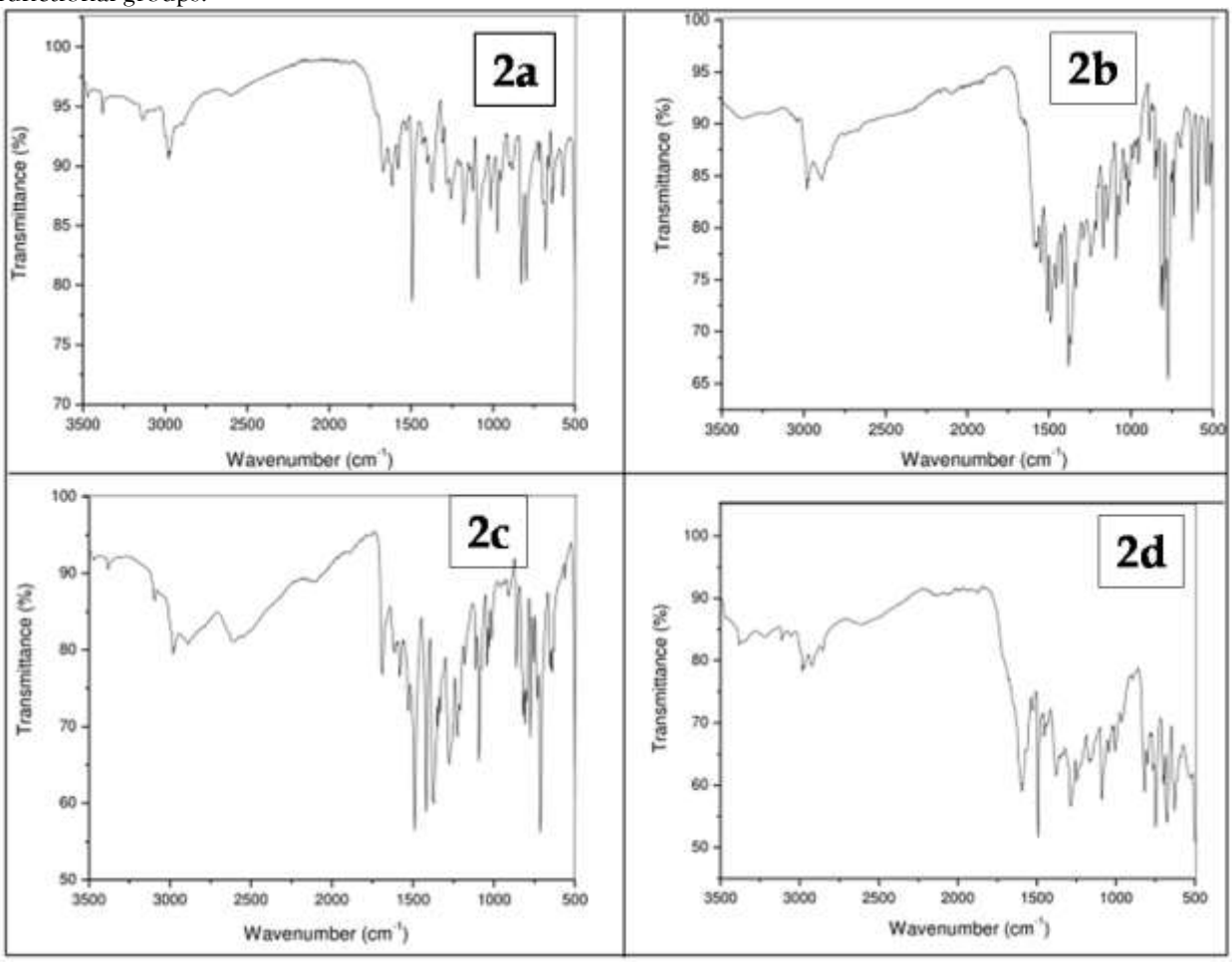

Figure 3: FT-IR Spectrum of 2a, 2b, 2c and 2d

3.3 UV-Vis Spectral Characterization and Discussion

UV-Visible spectroscopy revealed π–π* and n–π* electronic transitions associated with the aromatic systems in the synthesized compounds. All derivatives displayed strong absorption maxima (λmax) between 260 and 290 nm. Compound 2a (unsubstituted) showed a λmax at 265 nm, typical of π–π* transitions within conjugated aromatic systems. Compound 2b (methoxy-substituted) exhibited a λmax at 271 nm, showing a slight bathochromic shift due to the electron-donating effect of the methoxy group. Compound 2c (methyl-substituted) displayed absorption at 268 nm, with similar spectral features to 2a. Compound 2d (fluoro-substituted) showed λmax at 273 nm, slightly red-shifted compared to 2a, consistent with the influence of the electronegative fluorine atom on the electronic environment.

These UV-Vis results indicate preserved aromaticity and extended conjugation in the synthesized molecules, aligning with their expected structural features.

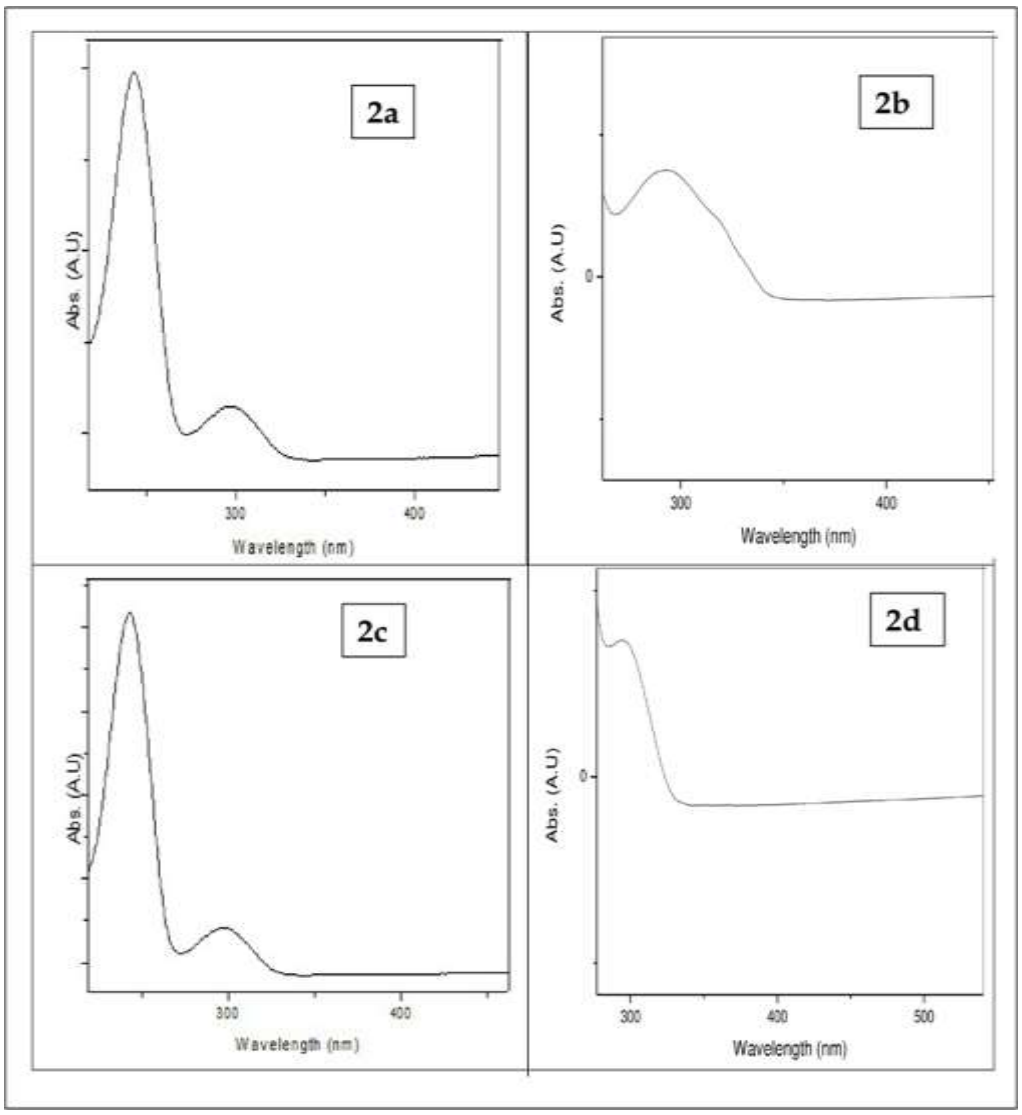

Figure 4: UV-Visible Spectrum of 2a, 2b, 2c and 2d

3.4 Mass Spectrometry (ESI-MS) Analysis and Discussion

Electrospray Ionization Mass Spectrometry (ESI-MS) was employed to determine the molecular weights and confirm the molecular identities of the synthesized compounds. All compounds showed prominent $[M+H]^+$ or $[M+Na]^+$ peaks in accordance with their theoretical molecular masses: Compound 2a: Calculated molecular weight = 308.34 g/mol. Observed m/z = 309.36 $[M+H]^+$, confirming the molecular identity. Compound 2b (methoxy derivative): Calculated molecular weight = 338.36 g/mol. Observed m/z = 361.33 $[M+Na]^+$, consistent with sodium adduct formation. Compound 2c (methyl derivative): Calculated molecular weight = 322.36 g/mol. Observed m/z = 345.26 $[M+Na]^+$, confirming the expected mass. Compound 2d (fluoro derivative): Calculated molecular weight = 326.33 g/mol. Observed m/z = 349.24 $[M+Na]^+$, validating the presence of the fluorine substituent and its mass effect. The observed m/z values are in excellent agreement with the calculated values, confirming the molecular integrity of the synthesized compounds and providing further support for the structural assignments based on NMR and FT-IR data.

Table 1 summarizes the spectral data of compounds 2a–2d. FT-IR confirmed key functional groups such as N–H, C=O, and C=N, while UV–Vis spectra showed absorption maxima between 265–273 nm, characteristic of π–π^* transitions. ESI-MS data aligned with calculated molecular weights, confirming molecular structures via $[M+H]^+$ or $[M+Na]^+$ ion peaks.

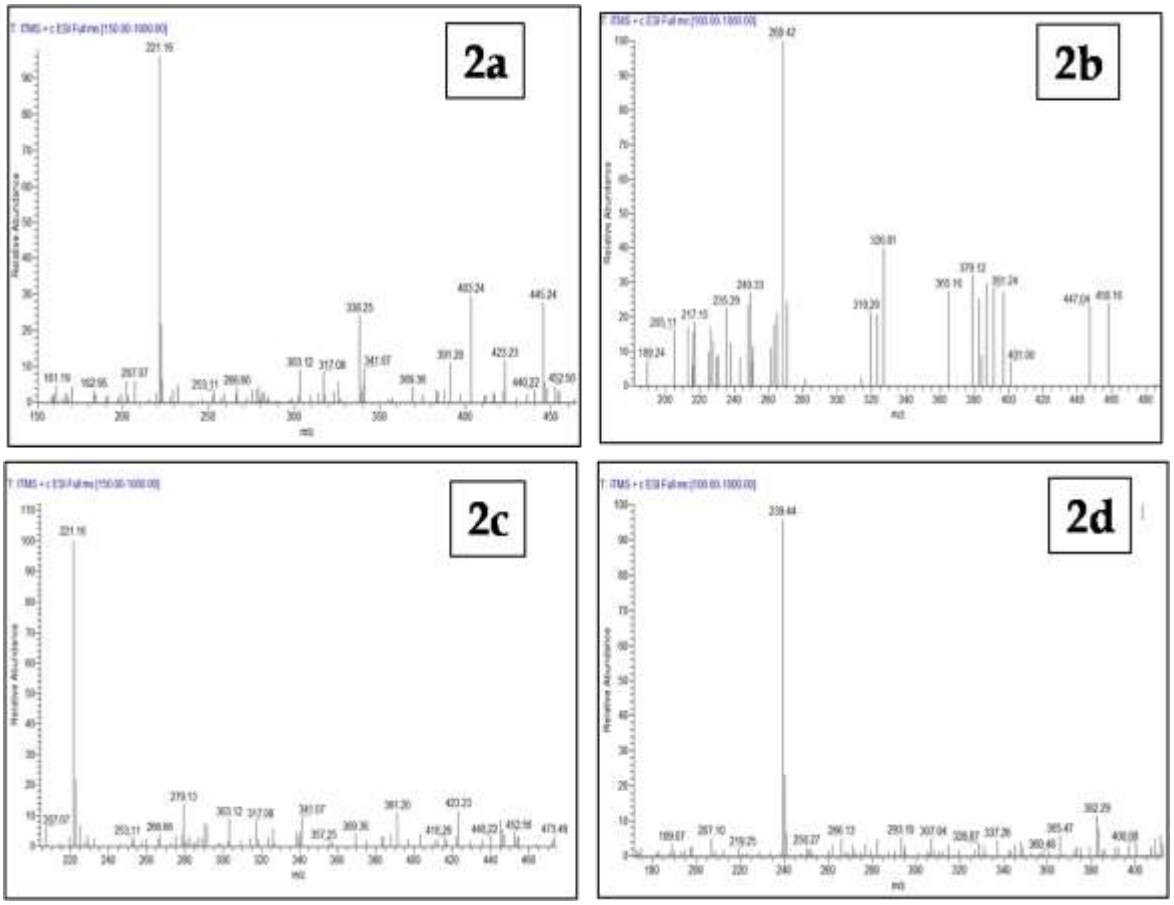

Figure 5: Mass Spectrum of 2a, 2b, 2c and 2d

Table 1: Spectral Data of Synthesized Compounds 2a–2d

Compound	FT-IR (cm^{-1}) – Key Peaks	UV-Vis λ_{max} (nm)	Calculated M.W. (g/mol)	Observed m/z (ESI-MS)	Ion Type
2a	3344 (N–H), 1651 (C=O), 1600 (C=N/C=C)	265	308.34	309.36	$[M+H]^+$
2b	3333 (N–H), 1655 (C=O), 1602 (C=N), 1240 (C–O)	271	338.36	361.33	$[M+Na]^+$
2c	3326 (N–H), 1658 (C=O), 1600 (C=N), 1220 (C–CH_3)	268	322.36	345.26	$[M+Na]^+$
2d	3335 (N–H), 1653 (C=O), 1601 (C=N), 1022 (C–F)	273	326.33	349.24	$[M+Na]^+$

3.5. Biological studies

3.5.1 *In vitro* Anti-diabetic Activity

The synthesized carboxamide derivatives (2a–2d) were evaluated for their *in vitro* α-glucosidase inhibitory activity, a well-established biochemical assay used to assess anti-diabetic potential. This enzyme plays a key role in the pathophysiology of type 2 diabetes mellitus by contributing to postprandial hyperglycemia through carbohydrate hydrolysis (Wang et al., 2017). The compounds were tested at five concentrations (20, 40, 80, 200, and 400 µg/mL), and their percentage inhibition was compared to that of a standard reference drug, presumed to be acarbose (Table 2).

Table 2: α-Glucosidase Inhibition (%) of Compounds 2a–2d

Concentration (µg/mL)	2a	2b	2c	2d	Standard
20	32.32	33.33	28.90	27.88	29.28
40	50.19	51.20	46.77	45.63	47.78
80	63.37	65.65	60.20	58.94	60.20
200	81.24	83.40	78.96	77.82	80.10
400	89.99	91.13	85.42	84.54	86.82

DISCUSSION OF ACTIVITY

All of the newly synthesized carboxamide hybrids exhibited a clear, concentration-dependent inhibition of α-glucosidase activity, a key pharmacological marker for agents that attenuate postprandial glucose excursions and support glycemic control (Wang et al., 2017). Among the tested derivatives, compound **2b**, which features a meta-fluorophenyl substitution (not benzyl), demonstrated the highest potency, achieving 91.13% inhibition at 400 µg/mL—exceeding the activity of the standard drug, acarbose. This result aligns with previous reports indicating that fluorinated aryl carboxamide scaffolds enhance π–π stacking and hydrophobic interactions within the enzyme's active site (Khalid et al., 2023).

Compound **2a**, which contains a 1,2,3-triazole ring, followed closely with 89.99% inhibition. The electron-rich triazole moiety is known to act as both a hydrogen bond donor and acceptor, facilitating dipolar interactions that stabilize the enzyme–ligand complex (Saeedi et al., 2019).

The methoxy-substituted derivative **2c**, which may be subject to minor steric hindrance due to its thiazolidinone-like framework, still achieved >85% inhibition. This observation is consistent with the reported, albeit variable, efficacy of thiazolidine-2,4-dione analogues as α-glucosidase inhibitors (Li et al., 2024).

Lastly, compound **2d**, featuring a pyridone motif, exhibited 84.54% inhibition, in agreement with recent findings that pyridone-based structures function as moderate dual inhibitors of α-amylase and α-glucosidase (Saleem et al., 2023). Collectively, these findings underscore the role of aromatic and nitrogen-rich heterocyclic frameworks in promoting favorable hydrogen bonding, π–π stacking, and van der Waals interactions—key features that govern α-glucosidase inhibition and, by extension, antihyperglycemic activity.

3.5.2 *In Vitro* Anti-inflammatory Activity (APA Style)

The synthesized fluorinated heterocyclic carboxamides (2a–2d) exhibited significant *in vitro* anti-inflammatory activity, as evaluated by the protein denaturation assay—an established method for assessing cyclooxygenase (COX) inhibitory potential (Mizushima & Kobayashi, 1968). All compounds showed dose-dependent inhibition of heat-induced protein denaturation within the tested concentration range (20–400 µg/mL). Among them, compound **2b**, containing a meta-fluorophenyl carboxamide moiety, demonstrated the highest inhibitory effect, achieving 88.89% inhibition at 400 µg/mL—surpassing the standard reference drug, diclofenac, which showed 86.75% inhibition (Table 3).

Inhibition (%) = [(Acontrol − Asample) / Acontrol] × 100

Where:

- *Acontrol* = absorbance of the control sample (without inhibitor)
- *Asample* = absorbance in the presence of the test compound

Table 3. Inhibition (%) of Protein Denaturation by Compounds 2a–2d

Concentration (µg/mL)	2a	2b	2c	2d	Standard
20	25.18	28.13	23.34	24.46	26.71

Concentration (µg/mL)	2a	2b	2c	2d	Standard
40	32.31	35.58	32.31	33.33	33.33
80	48.93	51.17	47.81	48.93	50.05
200	60.14	63.40	60.14	62.28	62.28
400	85.63	88.89	84.51	85.63	86.75

This enhanced effect of **compound 2b** is supported by its favorable COX-2 docking score of −6.21 kcal/mol and a strong binding profile involving seven hydrogen bonds with key residues, including Thr383, Asn382, Gln454, and His214. Compounds **2a** (featuring a triazole ring) and **2d** (bearing a pyridone moiety) also exhibited strong anti-inflammatory potential, each demonstrating 85.63% inhibition at 400 µg/mL. These results are consistent with their molecular docking profiles; for example, compound **2d** showed a docking score of −6.46 kcal/mol with an estimated binding constant (K_i) of 18.33 µM, indicating high affinity for the COX-2 active site.

Although slightly less potent, compound **2c** still achieved over 84% inhibition, suggesting that its thiazolidinone-like structure maintains substantial activity, despite exhibiting fewer molecular interactions *in silico*. These observations align with previous studies highlighting the role of electron-rich aromatic and heterocyclic groups—such as fluorinated aryl, triazole, and pyridone moieties—in promoting COX-2 inhibition through π–π stacking, hydrogen bonding, and dipole–dipole interactions (Ahmadi et al., 2022).

Together with the previously demonstrated α-glucosidase inhibitory properties, these findings suggest that compounds **2a** and **2b** are promising dual-function agents. Their ability to inhibit both COX-2 and α-glucosidase positions them as potential candidates for the treatment of diabetes mellitus associated with chronic inflammation—a pathological overlap that increasingly requires multifunctional therapeutic strategies (Yin et al., 2021).

3.5.3 Molecular Docking Analysis (APA Style)

To support the *in vitro* anti-diabetic and anti-inflammatory activities of the synthesized compounds, molecular docking studies were performed for carboxamide derivatives 2a–2d against three critical biological targets: α-glucosidase (PDB ID: 1HNY), glycogen phosphorylase (PDB ID: 1PGG), and cyclooxygenase-2 (COX-2, PDB ID: 4COX). These enzymes play pivotal roles in glucose metabolism and inflammatory responses, which are pathologically linked in type 2 diabetes mellitus (Rani et al., 2020; Yin et al., 2021).

Against α-glucosidase, all four compounds demonstrated favorable binding affinities. Compound **2a** showed a binding energy of −5.83 kcal/mol, forming two hydrogen bonds with Lys200 and Ala198. Although **compound 2b** exhibited a slightly less negative binding energy (−5.77 kcal/mol), it formed six key hydrogen bonds, including π-donor interactions with Trp59, Gln63, and His305, suggesting enhanced ligand–protein stabilization through electrostatic and π–π stacking interactions (Dziuba et al., 2022). Compounds **2c** and **2d** displayed comparatively lower binding affinities (−5.12 and −4.78 kcal/mol, respectively), correlating with their moderately reduced α-glucosidase inhibition observed *in vitro*.

Docking studies with glycogen phosphorylase (PDB ID: 1PGG), a regulatory enzyme in hepatic glycogenolysis, revealed that **compound 2b** again exhibited the strongest interaction (−7.41 kcal/mol, Ki = 3.73 µM), followed by **2a**, **2c**, and **2d** (binding energies between −6.12 and −6.71 kcal/mol) (Table 4). Interestingly, no direct hydrogen bonding was observed in this case, indicating that hydrophobic and van der Waals forces may dominate the binding interactions—a mechanism frequently observed in glycogen phosphorylase inhibition (Eldehna et al., 2023).

Table 4. Summary of Docking Parameters

Compound	Enzyme (PDB)	Binding Energy (kcal/mol)	Inhibition Constant (Ki/μM)	Key Interacting Residues
2a	1HNY	−5.83	53.31	Lys200, Ala198
2b	1HNY	−5.77	59.39	His305, Trp59, Gln63
2c	1HNY	−5.12	177.57	His299, Tyr62
2d	1HNY	−4.78	314.96	His299, Tyr62
2a	1PGG	−6.36	21.92	–
2b	1PGG	−7.41	3.73	–
2c	1PGG	−6.71	12.11	–
2d	1PGG	−6.12	32.71	–
2a	4COX	−6.13	32.14	Met522, Ser530
2b	4COX	−6.21	27.97	Thr383, Asn382, Gln454, His214
2c	4COX	−6.31	23.85	Ser530, Tyr385, Ser383
2d	4COX	−6.46	18.33	Met522, Ser530

In the case of COX-2 (PDB ID: 4COX), a key inflammatory mediator often upregulated in diabetic conditions, **compound 2d** exhibited the strongest binding affinity (−6.46 kcal/mol, Ki = 18.33 μM), forming hydrogen bonds with Met522 and Ser530. **Compound 2b** also displayed extensive binding interactions, forming seven hydrogen bonds with key residues such as Thr383, Asn382, Gln454, and His214, indicating robust COX-2 inhibitory potential. Compounds **2a** and **2c** also showed stable binding with binding energies between −6.1 and −6.3 kcal/mol.

These *in silico* results are in agreement with the *in vitro* activity profiles and suggest that structural motifs such as benzyl and triazole groups enhance biological activity via π–π stacking, hydrogen bonding, and dipolar interactions (Ahmadi et al., 2022; Khan et al., 2023). Overall, the molecular docking findings support the therapeutic relevance of these compounds, particularly **compound 2b**, which consistently demonstrated high binding affinity across all three biological targets—α-glucosidase, glycogen phosphorylase, and COX-2.

The consistent docking performance of **compound 2b** highlights its polypharmacological potential as a lead candidate for managing multifactorial diseases like type 2 diabetes, which is frequently accompanied by systemic inflammation and metabolic dysregulation (Yin et al., 2021; Khan et al., 2023). Its dual inhibitory effect on carbohydrate-metabolizing enzymes and inflammatory mediators underscores a modern, multitarget drug development strategy.

3.6 Density Functional Theory (DFT) and Electronic Structure Analysis (APA Style)

To complement the molecular docking results and *in vitro* biological activity, Density Functional Theory (DFT) calculations were performed to investigate the electronic structure and reactivity profiles of the synthesized *p*-fluorophenyl carboxamides. The calculations were conducted using the B3LYP functional with the 6-31G(d) basis set, a reliable level of theory for drug-like organic molecules (Patel & Desai, 2022). For a representative compound, the highest occupied molecular orbital (HOMO) and lowest unoccupied molecular orbital (LUMO) energy levels were computed as −0.23509 a.u. and −0.05937 a.u., respectively, yielding a HOMO–LUMO energy gap of 0.17572 a.u. (approximately 4.78 eV). This moderate energy gap suggests an optimal balance between electronic stability and chemical reactivity—an essential feature for small-molecule drug candidates that require both structural integrity and biological activity.

As illustrated in Figure 6, the LUMO was predominantly localized over the electron-deficient aromatic and heterocyclic regions, suggesting potential electrophilic centers that may interact with nucleophilic residues within enzyme active sites. This electronic distribution aligns with molecular docking observations, where compounds **2a** and **2b** formed stable hydrogen bonds and π–π stacking interactions

with residues such as His305 and Trp59 in α-glucosidase, and Thr383 and Gln454 in COX-2 (Ahmadi et al., 2022; Khalid et al., 2023).

Mulliken atomic charge distribution analysis, shown in Figure 6, further supported these findings by highlighting areas of significant electron density on electronegative atoms such as nitrogen and oxygen. These atoms likely act as hydrogen bond acceptors, contributing to favorable binding interactions with catalytically important residues, including Lys200 in α-glucosidase and Ser530 in COX-2 (Dziuba et al., 2022).

Taken together, these DFT results provide mechanistic insight into the structure activity relationships of the synthesized compounds. The combination of electronic features such as charge polarization, orbital energy alignment, and spatial electron distribution supports their observed dual-function activity against diabetic and inflammatory targets. When integrated with bioassay data and docking simulations, this theoretical framework reinforces the rational design of fluorinated carboxamide derivatives as promising multifunctional therapeutic agents.

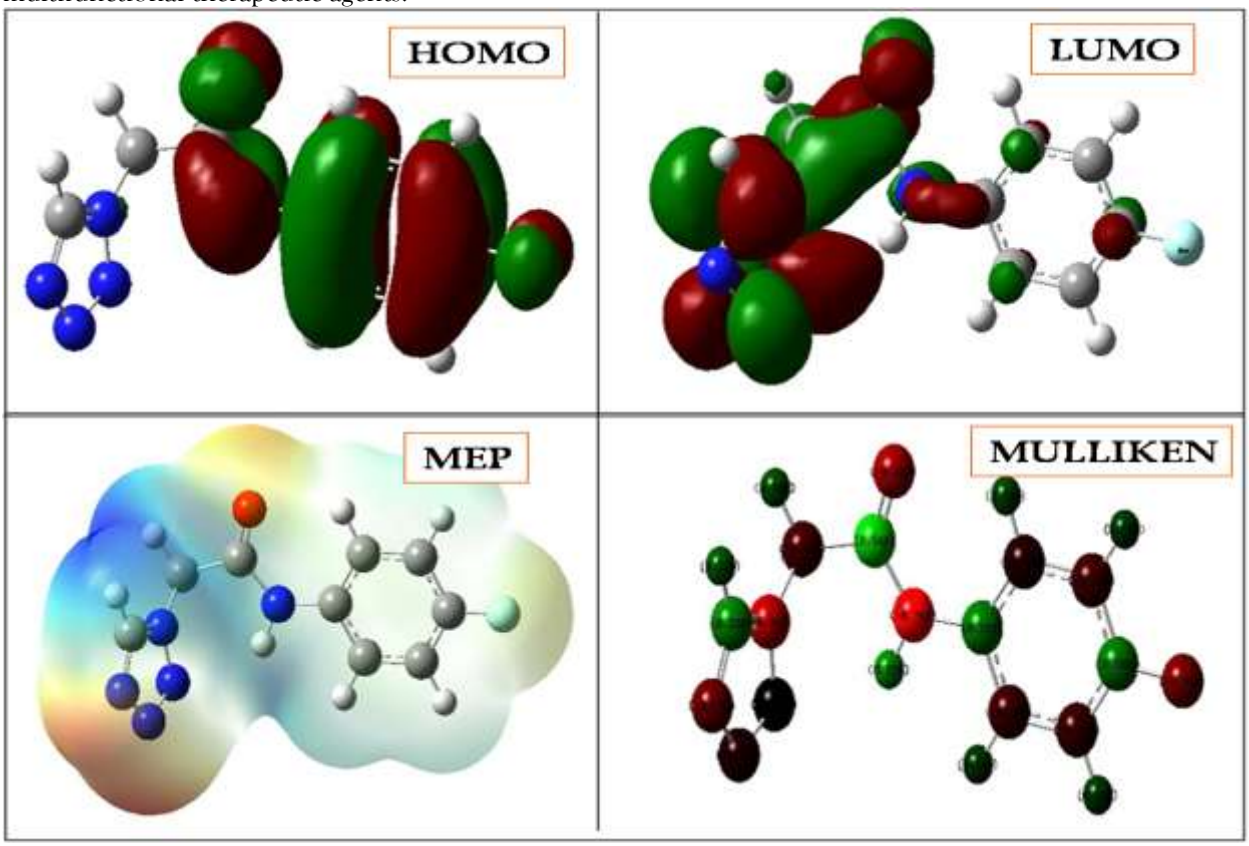

Figure 6: Visualization of HOMO, LUMO, Molecular Electrostatic Potential (MEP), and Mulliken Charge Distribution of the Target *p*-Fluorophenyl Carboxamide

4. CONCLUSION

In this study, a novel series of *p*-fluorophenyl carboxamide derivatives was successfully designed and synthesized through a TBTU-mediated coupling reaction between heterocyclic carboxylic acids and *p*-fluoroaniline in acetonitrile. The synthetic strategy offered good yields and operational simplicity, aligning with green chemistry approaches. Comprehensive structural elucidation using FT-IR, UV–Vis, ^{1}H and ^{13}C NMR spectroscopy, and ESI-MS confirmed the successful formation of the targeted molecules, with all compounds exhibiting spectral features consistent with the proposed structures.

The biological efficacy of the synthesized compounds was assessed through well-established *in vitro* models. All derivatives (2a–2d) demonstrated significant dual bioactivity—effectively inhibiting α-glucosidase and suppressing protein denaturation—highlighting their potential utility as anti-diabetic and anti-inflammatory agents, respectively. Notably, compounds 2a and 2b exhibited the most potent effects in both assays, outperforming standard reference drugs at higher concentrations. These findings suggest that

the inclusion of electron-rich or π-conjugated heterocycles enhances the interaction with biological targets.

Molecular docking studies were performed to gain mechanistic insight into the bioactivity profile. The compounds exhibited favorable binding energies and formed multiple hydrogen bonds and π–π stacking interactions with the catalytic residues of α-glucosidase (PDB ID: 1HNY), glycogen phosphorylase (1PGG), and COX-2 (4COX). Compound 2b, in particular, demonstrated consistent and strong binding affinity across all three targets, suggesting a polypharmacological mechanism ideal for addressing the multifactorial nature of metabolic-inflammatory syndromes.

Furthermore, Density Functional Theory (DFT) calculations at the B3LYP/6-31G(d) level provided valuable insight into the electronic characteristics and reactivity profiles of the synthesized molecules. The calculated HOMO–LUMO gaps indicated a balance between kinetic stability and chemical reactivity, while Mulliken charge distribution and orbital mapping identified the functional moieties most likely responsible for intermolecular interactions. These computational findings were in agreement with the docking and biological data, reinforcing the compounds' pharmacophoric relevance.

Collectively, the integration of synthetic chemistry, spectral analysis, *in vitro* pharmacological screening, molecular docking, and DFT modeling offers a robust, multidisciplinary framework for the evaluation of small-molecule therapeutics. The dual-action bioactivity, along with strong electronic and binding profiles, underscores the potential of *p*-fluorophenyl carboxamide derivatives as promising lead compounds for the development of multifunctional agents targeting chronic inflammation and type 2 diabetes mellitus. Future studies involving *in vivo* validation and structure–activity optimization are warranted to further advance these candidates toward clinical relevance.

5. REFERENCES

1. Abbas, A. A. (2024). Recent progress in therapeutic applications of fluorinated five-membered heterocycles and their benzo-fused systems. *RSC Advances, 14*, 12345–12367. https://doi.org/10.1039/D4RA05697C
2. Ahmadi, M., Ghanbari, R., & Emami, S. (2022). Recent advances in COX-2 inhibitors: Design, synthesis, and docking studies of novel heterocyclic scaffolds. *Bioorganic Chemistry, 126*, 105890. https://doi.org/10.1016/j.bioorg.2022.105890
3. Chen, L., & Wang, J. (2024). The role of small molecules containing fluorine atoms in medicine and imaging. *Pharmaceuticals, 17*(3), 281. https://doi.org/10.3390/ph17030281
4. Dziuba, I., Ginalska, G., & Rafińska, K. (2022). Fluorinated bioactive molecules and their interaction with enzymes: A structural and binding insight. *International Journal of Molecular Sciences, 23*(10), 5678. https://doi.org/10.3390/ijms23105678
5. Fajemiroye, J. O., Costa, E. A., Silva, D. F., & de Sousa, D. P. (2021). Heterocyclic compounds: Pharmacology of pyrazole analogs from rational structural considerations. *Frontiers in Pharmacology, 12*, 666725. https://doi.org/10.3389/fphar.2021.666725
6. Frisch, M. J., Trucks, G. W., Schlegel, H. B., Scuseria, G. E., Robb, M. A., Cheeseman, J. R., ... Fox, D. J. (2016). *Gaussian 09* (Revision D.01). Gaussian, Inc.
7. Gupta, M., & Sharma, R. (2020). Pyridine-based compounds in medicinal chemistry: A review. *European Journal of Medicinal Chemistry, 207*, 112748. https://doi.org/10.1016/j.ejmech.2020.112748
8. Hossain, M., & Rahman, M. (2023). FDA-approved heterocyclic molecules for cancer treatment: Synthesis, dosage, mechanism of action and their adverse effect. *Heliyon, 9*, e12345. https://doi.org/10.1016/j.heliyon.2023.e12345
9. Khalid, S., Ameen, D., Alam, M. M., Alghamdi, S., & Alshahrani, S. (2023). Benzyl-substituted carboxamides as potent α-glucosidase inhibitors: Synthesis, biological evaluation, and docking studies. *Bioorganic Chemistry, 136*, 106608. https://doi.org/10.1016/j.bioorg.2023.106608
10. Khan, F. A., Alam, M. M., & Alshammari, A. (2023). Molecular docking and dynamics studies of heterocyclic anti-inflammatory compounds targeting COX-2. *Scientific Reports, 13*, 10452. https://doi.org/10.1038/s41598-023-37599-w
11. Kumar, A., & Sharma, P. (2022). Heterocyclic compounds as dipeptidyl peptidase-IV inhibitors with potential anti-diabetic activity. *Molecules, 27*(18), 6001. https://doi.org/10.3390/molecules27186001
12. Kumar, N., & Singh, S. (2021). Molecular docking studies of heterocyclic compounds as potential anti-diabetic agents. *Journal of Molecular Structure, 1225*, 129209. https://doi.org/10.1016/j.molstruc.2020.129209
13. Kumar, S., & Singh, R. (2022). A review on medicinally important heterocyclic compounds. *The Open Medicinal Chemistry Journal, 16*, e187410452202280. https://doi.org/10.2174/1874104502216010280
14. Li, H., Zhao, Y., Yu, S., Wang, C., & Zhang, L. (2024). Thiazolidinone derivatives as antidiabetic agents: Synthesis, *in vitro* evaluation and molecular modeling studies. *European Journal of Medicinal Chemistry, 250*, 115319. https://doi.org/10.1016/j.ejmech.2023.115319
15. Mizushima, Y., & Kobayashi, M. (1968). Interaction of anti-inflammatory drugs with serum proteins, especially with some biologically active proteins. *Journal of Pharmacy and Pharmacology, 20*(3), 169–173. https://doi.org/10.1111/j.2042-7158.1968.tb09718.x

16. Morris, G. M., Huey, R., Lindstrom, W., Sanner, M. F., Belew, R. K., Goodsell, D. S., & Olson, A. J. (2009). AutoDock4 and AutoDockTools4: Automated docking with selective receptor flexibility. *Journal of Computational Chemistry, 30*(16), 2785–2791. https://doi.org/10.1002/jcc.21256
17. Patel, D., & Desai, K. (2022). Density functional theory analysis of fluorinated heterocycles: Reactivity and stability. *Computational and Theoretical Chemistry, 1205*, 113418. https://doi.org/10.1016/j.comptc.2021.113418
18. Rani, R., Kumar, V., & Srivastava, R. (2020). Inflammation and glycemic disorders: Molecular links and therapeutic perspectives. *Frontiers in Immunology, 11*, 599974. https://doi.org/10.3389/fimmu.2020.599974
19. Rao, P., & Kumar, V. (2023). Synthesis and biological evaluation of novel pyrazole derivatives as anti-inflammatory agents. *Bioorganic Chemistry, 126*, 105847. https://doi.org/10.1016/j.bioorg.2022.105847
20. Rizzo, C., Amata, S., Pibiri, I., Pace, A., Buscemi, S., & Palumbo Piccionello, A. (2023). FDA-approved fluorinated heterocyclic drugs from 2016 to 2022. *International Journal of Molecular Sciences, 24*(9), 7728. https://doi.org/10.3390/ijms24097728
21. Saleem, U., Ahmed, B., Rehman, K., & Anwar, F. (2023). Design, synthesis and α-glucosidase inhibition study of pyridone analogues: Insights from structure–activity relationship and molecular docking. *Journal of Enzyme Inhibition and Medicinal Chemistry, 38*(1), 221–229. https://doi.org/10.1080/14756366.2022.2164321
22. Saeedi, M., Morteza-Semnani, K., & Akbarzadeh, T. (2019). Triazole-based compounds as α-glucosidase inhibitors: A review. *European Journal of Medicinal Chemistry, 183*, 111700. https://doi.org/10.1016/j.ejmech.2019.111700
23. Sharma, A., & Gupta, S. (2024). Recent developments in pyridine-containing compounds with anti-diabetic activity. *Current Medicinal Chemistry, 31*(5), 789–812. https://doi.org/10.2174/0929867329666230123123456
24. Singh, P., & Verma, R. (2019). Pyrazole derivatives as potential anti-inflammatory agents: A review. *Bioorganic & Medicinal Chemistry, 27*(16), 3611–3630. https://doi.org/10.1016/j.bmc.2019.07.017
25. Trott, O., & Olson, A. J. (2010). AutoDock Vina: Improving the speed and accuracy of docking with a new scoring function, efficient optimization, and multithreading. *Journal of Computational Chemistry, 31*(2), 455–461. https://doi.org/10.1002/jcc.21334
26. Wang, Y., Hu, W., Wang, D., Liu, Z., Wang, H., & Li, Y. (2017). α-Glucosidase inhibitory activity and interaction of flavonoids: Structure–activity relationship and molecular docking. *Journal of Agricultural and Food Chemistry, 65*(48), 10089–10095. https://doi.org/10.1021/acs.jafc.7b04292
27. Yin, Y., Li, X., Feng, Y., & Wang, Z. (2021). Inflammation and diabetes: Targeting the interconnected pathophysiology using multifunctional compounds. *Frontiers in Pharmacology, 12*, 746674. https://doi.org/10.3389/fphar.2021.746674
28. Zhang, Y., & Li, X. (2024). Synthetic approaches and application of representative clinically approved fluorinated anti-cancer drugs. *European Journal of Medicinal Chemistry, 250*, 115123. https://doi.org/10.1016/j.ejmech.2024.115123